Physics of Atomic Nuclei, Vol. 68, No. 2, 2005, pp. 191–207. Translated from Yadernaya Fizika, Vol. 68, No. 2, 2005, pp. 216–232.

NUCLEI
Theory

Investigation of the Neutron Shell Structure of the Even–Even Isotopes $^{40-56}$Ca within the Dispersive Optical Model

O. V. Bespalova*, I. N. Boboshin, V. V. Varlamov, T. A. Ermakova, B. S. Ishkhanov, E. A. Romanovsky, T. I. Spasskaya, and T. P. Timokhina

Institute of Nuclear Physics,
Moscow State University, Vorob'evy gory, Moscow, 119899 Russia

Received December 3, 2003; in final form, May 1, 2004

Abstract—Within the method of matching experimental data obtained in the neutron-stripping and neutron-pickup reactions on ^{40,42,44,46,48}Ca isotopes, the single-particle energies and probabilities that neutron states are filled are obtained for the even–even calcium isotopes. These data are analyzed within the dispersive optical model, and good agreement between the calculated and experimental values of the energies of states is obtained. The dispersive optical potential is extrapolated to the region of the unstable ^{50,52,54,56}Ca nuclei. The calculated single-particle energies of bound states in these isotopes are compared with the results of the calculations within the multiparticle shell model, the latter predicting a new magic number $N = 34$ for $Z = 20$ nuclei. © *2005 Pleiades Publishing, Inc.*

1. INTRODUCTION

Searches for and investigation of new magic nuclei form one of the most important lines of experimental and theoretical studies stimulated by advances in the realms of obtaining and accelerating radioactive nuclei and by the development of new computational procedures in nuclear-structure theory.

In the past years, a full set of parameters of effective interaction for pf-shell nuclei has been determined on the basis of experimental information about the energies of single-particle states and matrix elements of two-particle interactions for the doubly magic nuclei $^{40}_{20}$Ca$_{20}$ and $^{48}_{20}$Ca$_{28}$ and nuclei closest to them. By using the new set of effective-interaction parameters, the energies of 2^+_1 states in the even–even calcium isotopes from ^{42}Ca to ^{56}Ca inclusive were calculated in [1] on the basis of the multiparticle shell model (MSM).

For the even–even calcium isotopes from the mass-number range $42 \le A \le 52$, the calculated energies of 2^+_1 states are in good agreement with their experimental counterparts. For ^{54}Ca, the calculated energy of the 2^+_1 state is identical to that in the ^{48}Ca nucleus, while its counterpart in ^{56}Ca is close to the energies of the 2^+_1 states in ^{42,44,46}Ca. Also, the single-particle energies of the $1f$ and $2p$ neutron states were calculated in [1] for the even–even nuclei $^{42-56}$Ca. It was shown that the energy gap between the $1f_{5/2}$ and $2p_{1/2}$ states increases as the mass number A grows from 50 to 54, reaching a value of about 4 MeV—that is, this gap proves to be commensurate with the gap between the $1f_{7/2}$ and $2p_{3/2}$ states in the doubly magic nucleus $^{48}_{20}$Ca$_{28}$. On the basis of the fact that the gap between the $1f_{5/2}$ and $2p_{1/2}$ states is correlated with the energy of the 2^+_1 level in ^{54}Ca, it was assumed in [1] that, in the ^{54}Ca nucleus, the $2p_{3/2}$ and $2p_{1/2}$ subshells are completely filled; therefore, $N = 34$ is a new magic number for $Z = 20$ isotopes, and the $^{54}_{20}$Ca$_{34}$ nucleus is a candidate for a doubly magic nucleus.

In order to test the assumption that the number $N = 34$ is magic, it is important to determine experimentally the energy of the first 2^+_1 level in the ^{54}Ca nucleus and to calculate the energy gap between the $1f_{5/2}$ and $2p_{1/2}$ states in the ^{50,52,54,56}Ca nuclei on the basis of a model that is different from the multiparticle shell model and which would make it possible to obtain reliable data on the single-particle energies E_{nlj} of neutron states specified by the quantum numbers n, l, and j.

However, it is necessary to assess the reliability of the experimental values of single-particle energies before proceeding to compare the results of respective calculations with them. We address this issue in the second section of this article. Our analysis of experimental data has made it possible to find, for the ^{40,42,44,46,48}Ca nuclei, sets of reliable experimental values of energies for single-particle states.

*e-mail: besp@monet.npi.msu.ru

In the third section of the article, the refined experimental data on the single-particle energies of states are compared with the results obtained by other authors on the basis of various models. For the ^{40}Ca nucleus, we analyze the quantities

$$\chi^2 = \sum_{nlj} \left(\frac{E^{\text{theor}}_{nlj} - \mathrm{E}^{\text{expt}}_{nlj}}{\Delta^{\text{expt}}_{nlj}} \right)^2,$$

where $\Delta^{\text{expt}}_{nlj}$ is the error in determining E^{expt}_{nlj} for states in the vicinity of the Fermi energy E_{F}. It is shown that minimum values of χ^2 correspond to the E^{DOM}_{nlj} values calculated within the dispersive optical model (DOM).

In the fourth section of the article, it is shown that the use of the traditional version of the dispersive optical model in calculating the energies of levels in the stable even–even isotopes $^{42-48}$Ca runs into serious difficulties because of scarcity of experimental data on neutron-scattering cross sections. In order to describe experimental information obtained for the single-particle properties of states of the ^{42,44,46,48}Ca nuclei, we therefore employ a new version of the dispersive optical model.

In the fifth section, we investigate the accuracy to which it is possible to match the single-particle energies calculated for neutron states in the ^{42,44,46,48}Ca nuclei on the basis of the new version of the dispersive optical model with their experimental counterparts. It is shown that, for valence states, the calculated and experimental values of the energies E_{nlj} agree within the experimental errors.

In the sixth section, we discuss issues associated with extrapolating some parameters of the dispersive optical potential from the region of stable nuclei to the region of unstable nuclei, present the results obtained by calculating the single-particle energies of neutron states for the ^{50,52,54,56}Ca nuclei, and explore the possible magicity of the number $N = 34$ in $Z = 20$ nuclei.

2. SINGLE-PARTICLE ENERGIES AND PROBABILITIES OF THE FILLING OF NEUTRON STATES IN ^{40,42,44,46,48}Ca

The parameters of the neutron shell structure of the ^{40,42,44,46,48}Ca nuclei in the vicinity of E_{F} were determined by the method based on matching the data obtained in stripping and pickup reactions on the same nucleus. The single-particle energies E_{nlj} of subshells characterized by the quantum numbers n, l, and j and their occupation numbers N_{nlj} were calculated with allowance for the spectroscopic factors S_{nlj}. A detailed description of this method is given in [2]. Below, we only present the formulas for calculating N_{nlj} and E_{nlj}.

For levels characterized by the energy E_x and the quantum numbers n, l, and j, we denote by $S^{\mp}_{nlj}(E_x)$ the spectroscopic factors determined from data on pickup $(-)$ and stripping $(+)$ reactions and by $S^{\mp}_{nlj}$ the total spectroscopic factors:

$$S^{-}_{nlj} = \sum_x S^{-}_{nlj}(E_x), \quad S^{+}_{nlj} = \sum_x S^{+}_{nlj}(E_x). \quad (1)$$

In Eq. (1), the quantity $S^{-}_{nlj}(E_x)$ is proportional to the number of particles in the respective subshell (in the case of a pickup reaction), while $S^{+}_{nlj}(E_x)$ is proportional to the number of vacancies in the subshell (in the case of a stripping reaction).

From the energies E_x of the levels and the quantities $S^{\mp}_{nlj}(E_x)$, one determines the energies of the centroids of single-particle levels in final nuclei:

$$e^{-}_{nlj} = \frac{\sum\limits_x E_x S^{-}_{nlj}(E_x)}{S^{-}_{nlj}}, \quad e^{+}_{nlj} = \frac{\sum\limits_x E_x S^{+}_{nlj}(E_x)}{S^{+}_{nlj}}. \quad (2)$$

A transition from the energies e^{-}_{nlj} and e^{+}_{nlj} reckoned from the ground-state energies of the final nuclei $(A-1)$ and $(A+1)$ to the energies E^{-}_{nlj} and E^{+}_{nlj} reckoned from the ground-state energy of the nucleus A is accomplished by the formulas

$$E^{-}_{nlj}(A) = -B(A) - e^{-}_{nlj}, \quad (3)$$

$$E^{+}_{nlj}(A+1) = -B(A+1) + e^{+}_{nlj}, \quad (4)$$

where $B(A)$ and $B(A+1)$ are the neutron-separation energies in the nuclei whose mass numbers are A and $A+1$, respectively.

For each nucleus, experimental information about the stripping and pickup of neutrons was recast into a mutually consistent form by renormalizing the spectroscopic factors in such a way that respective sum rules were valid for them. The renormalized values of $\mathbf{S}^{\mp}_{nlj}$ were used to calculate the average occupation numbers for single-particle states by the formula

$$N_{nlj} = \frac{[\mathbf{S}^{-}_{nlj} + (2j+1-\mathbf{S}^{+}_{nlj})]}{2(2j+1)}. \quad (5)$$

The single-particle energies E_{nlj} of states were determined from the relation

$$E_{nlj} = \frac{\mathbf{S}^{-}_{nlj}E^{-}_{nlj} + \mathbf{S}^{+}_{nlj}E^{+}_{nlj}}{\mathbf{S}^{-}_{nlj} + \mathbf{S}^{+}_{nlj}}. \quad (6)$$

From Eqs. (3)–(6), we obtain

$$-E_{nlj} = (1 - N_{nlj})[B(A+1) - e^{+}_{nlj}] + N_{nlj}[B(A) + e^{-}_{nlj}]. \quad (7)$$

In order to determine N_{nlj} and E_{nlj}, we used the experimental data on the reactions of neutron stripping and pickup from [3–6; 7–10; 4, 8, 11, 12; 13–17; 18–22] for ^{40}Ca, ^{42}Ca, ^{44}Ca, ^{46}Ca, and ^{48}Ca, respectively.

The spins of the levels in the $^{A-1}$Ca and $^{A+1}$Ca nuclei were borrowed from the "Adopted Levels" section of the ENSDF international database of nuclear properties [23]. For a large number of levels excited in $^{A-1}$Ca and $^{A+1}$Ca nuclei in the pickup and stripping reactions, the spin values are ambiguous or unknown; therefore, the calculation was performed for each possible spin value. For the sake of brevity, the set of E_{nlj} values found from such calculations will be referred to as a "solution." An analysis of all solutions makes it possible to determine the total range of energies and occupation numbers for each single-particle state.

It is well known that $S_{nlj}(E_x)$ values calculated by the distorted-wave method involve an uncertainty not less than 20%, which contains both a systematic and a statistical component. The first is caused by the method used to derive spectroscopic factors as the coefficients of proportionality between the experimental values of the cross sections and their counterparts calculated by the distorted-wave method. Calculations within the distorted-wave method are based on the use of standard codes, the geometric parameters of the real and spin–orbit potentials being fixed, as a rule. The depth of the real potential is determined for each state. The calculations reveal that a 1% variation in the range parameter of the Woods–Saxon (WS) real potential for the $n + A$ system leads to a change of 10% in the calculated differential cross section for the stripping or pickup reaction. The systematic uncertainty in $S_{nlj}(E_x)$ also receives contributions from the ambiguities in the parameters of the optical potentials for projectile and emitted particles, uncertainties in the effective nucleon–nucleus interaction, and uncertainties in the sum rule. The application of the method based on matching data on stripping and pickup reactions makes it possible to remove, to a considerable extent, these sources of systematic uncertainties, the remaining statistical uncertainty in determining the individual values of renormalized $\mathbf{S}_{nlj}(E_x)$ being estimated at a value not greater than 10%. The errors in N_{nlj} values are about 0.05 near their boundaries of 0 and 1, falling to about 0.1 between their boundaries [2]. The use of the sums of the spectroscopic factors in our calculations creates a new source of uncertainties, since the quantum number j is unknown for many spectroscopic factors, so that the inclusion of such a spectroscopic factor in the sum in (1) or (2) or the disregard of this form factor would change the value of the respective sum. The method used in our analysis makes it possible to estimate these uncertainties by sampling all of the acceptable values of j. Therefore, the total error in determining $\mathbf{S}_{nlj}$ and N_{nlj} is taken here to be a root-mean-square value that takes into account the error because of the uncertainty in the spins of states and an error of about 10% in determining the individual values of renormalized $\mathbf{S}_{nlj}$. The errors in the single-particle energies are determined in a similar way.

The N_{nlj} and E_{nlj} values found for ^{40,42,44,46,48}Ca are given in Table 1, along with their total errors in parentheses. One can see that, because of incompleteness of experimental data, we were unable to determine the features of some states. The values N^{expt}_{nlj} and E^{expt}_{nlj} quoted in Table 1 for single-particle states in the vicinity of E_{F} for the ^{40,42,44,46,48}Ca isotopes were determined by using a unified method for all nuclei and are the most complete data. We note that, here, we define single-particle energies with allowance for coupling to collective degrees of freedom, which affect the occupation numbers for single-particle states and the energy centroids appearing in Eq. (7).

Figure 1 shows, according to data in Table 1, the energy positions of single-particle neutron orbits in calcium nuclei. From this figure, one can see that an increase in the number of neutrons in the $1f_{7/2}$ subshell leads to an increase in the absolute value of the energy of the $1f_{7/2}$ state and to a modest decrease in the absolute value of the energy of the $2p_{3/2}$ state, with the result that an individual shell in $^{48}_{20}\text{Ca}_{28}$ and the magic number $N = 28$ appear.

The single-particle energy E_{nl} of the state characterized by the quantum numbers n and l can be expressed in terms of spin–orbit splitting $\Delta_{\text{so}}(nl) = E_{nlj=l-1/2} - E_{nlj=l+1/2}$ as

$$E_{nl} = E_{nlj=l-1/2} - \Delta_{\text{so}}(nl)\frac{l+1}{2l+1}, \quad (8)$$

$$E_{nl} = E_{nlj=l+1/2} + \Delta_{\text{so}}(nl)\frac{l}{2l+1}.$$

According to the data in Table 1, the values of E_{nl} for the $1f$ states in ^{40}Ca, ^{46}Ca, and ^{48}Ca are -4.92, -6.70, and -6.44 MeV, respectively, while the corresponding values for the $2p$ states are -5.49, -5.09, and -4.08 MeV. With increasing number of neutrons in calcium isotopes, the energy gap between the p and f states proves to be approximately four times larger in ^{48}Ca than in ^{40}Ca. As N increases from 20 to 28, the energy gap between the $2p_{3/2}$ and $1f_{7/2}$ subshells increases approximately in the same proportion.

Table 1. Mean neutron occupation numbers N_{nlj} for subshells in the ^{40,42,44,46,48}Ca nuclei and their single-particle energies $-E_{nlj}$ (in MeV)

Subshell	N_{nlj}	$-E_{nlj}$	N_{nlj}	$-E_{nlj}$	N_{nlj}	$-E_{nlj}$	N_{nlj}	$-E_{nlj}$	N_{nlj}	$-E_{nlj}$
	^{40}Ca		^{42}Ca		^{44}Ca		^{46}Ca		^{48}Ca	
$2s_{1/2}$	>0.92	17.2(18)	0.93(4)	15.44(154)					1.00(0)	15.07(152)
$1d_{3/2}$	0.83(3)	15.2(20)	0.91(4)	13.03(184)	0.94(6)	13.91(159)			0.99(1)	15.22(179)
$1f_{7/2}$	0.02(2)	7.52(75)	0.20(4)	7.70(107)	0.49(8)	9.23(112)	0.77(7)	10.07(100)	1.00(0)	10.10(101)
$2p_{3/2}$	0.02(2)	6.10(67)	0.01(0)	5.73(57)	0.07(3)	5.92(75)	0.10(5)	5.84(60)	0.01(1)	4.68(47)
$2p_{1/2}$	0.01(1)	4.27(43)	0.00(0)	4.10(41)	0.01(0)	3.63(36)	0.04(4)	3.58(39)	0.00(0)	2.87(28)
$1f_{5/2}$	0.02(2)	1.46(20)					0.06(5)	2.20(45)	0.03(3)	1.57(40)

On the basis of data quoted in Table 1, one can trace variations in the particle–hole gap $\Delta^{\text{expt}} = E_{1f_{7/2}} - E_{1d_{3/2}}$ for the ^{40,42,44,46}Ca nuclei. The gap value of $\Delta^{\text{expt}} = E_{2p3/2} - E_{1f7/2} = 5.42(111)$ MeV for ^{48}Ca is smaller than Δ^{expt} for ^{40}Ca approximately by 2 MeV.

From the data in Table 1, it follows that, for ^{40,42}Ca, the sequence of the levels is $2s_{1/2}$–$1d_{3/2}$, while, for ^{48}Ca, there is an experimental indication that the sequence of the levels changes to become $1d_{3/2}$–$2s_{1/2}$, but the uncertainties in E_{nlj}^{expt} give no way to draw a definitive conclusion. Calculations on the basis of the relativistic mean-field approximation (RMFA) [24, 25] predict the sequence $1d_{3/2}$–$2s_{1/2}$, while the results reported in [26–28] favor the inverse sequence $2s_{1/2}$–$1d_{3/2}$.

It seems necessary to compare the data on E_{nlj}^{expt} for $^{40-48}$Ca in Table 1 with those that are available in the literature. In Table 2, we quote data on E_{nlj}^{expt} for the $2s_{1/2}$, $1d_{3/2}$, $1f$, and $2p$ states in the ^{40,48}Ca nuclei from articles in which the compiled values of E_{nlj}^{expt} are contrasted against E_{nlj}^{theor}.

From an analysis of the data on E_{nlj}^{expt} (see Tables 1, 2) for ^{40}Ca, it follows that the average value found in the present study for the energy of the $2s_{1/2}$ state is smaller in absolute value than its counterpart quoted in [5, 29–33] approximately by 1 MeV. It should be noted that, in those studies, only the ^{39}Ca state at $E_x = 2.463$ MeV, which possesses the highest spectroscopic factor, was taken into account in determining the energy of the $2s_{1/2}$ level. A modest distinction between the average energy of the $1d_{3/2}$ state and that which is given in [5, 29, 31–33] is explained in a similar way. From Table 2, it can be seen that, according to data from [5, 29–33], the spacing between the $1f_{7/2}$ and $2p_{3/2}$ levels lies in the range 1.9–2.5 MeV; according to our data, it is as small as 1.4 MeV. It is noteworthy that our result for the central value of the single-particle energy of the $1f_{7/2}$ state in the ^{40}Ca nucleus is approximately 0.8 MeV less than its counterparts in other studies. This is explained by taking here into account the fragmentation of the stripping strength for the $1f_{7/2}$ state and its distribution over various states of the ^{41}Ca nucleus. The use of full arrays of data on the spin–parities of the ^{41}Ca nucleus made it possible to conclude that the $1f_{7/2}$ spectroscopic strength is distributed among several states, including, in addition to the ground state, at least three more states of ^{41}Ca at 6567.4, 6686.2, and 6748.1 keV. Because of the fragmentation of the $1f_{7/2}$ state, the centroids of the $1f_{7/2}$ and $2p_{3/2}$ states prove to be quite close to each other, so that the corresponding occupation numbers are identical (see Table 1). We also note that our result for the energy of the $1f_{5/2}$ state is consistent with the data from [5], but that it is two times less in absolute value than the result quoted in [31] and 2.5 times less than its counterpart in [32].

Table 2 presents the values E_{nlj}^{expt} for ^{48}Ca from [29, 33]. We note that, within the errors, the energies of the $1f$ and $2p$ states from [29, 33] agree with our results, but that the energies of the $2s_{1/2}$ and $1d_{3/2}$ states according to our data are much greater in absolute value than their counterparts in those studies. With allowance for what will be said in the next section, the data on E_{nlj}^{theor} in the vicinity of E_{F} that were calculated for $^{40-48}$Ca by different authors within various theoretical approaches will be compared with the values E_{nlj}^{theor} obtained in the present study.

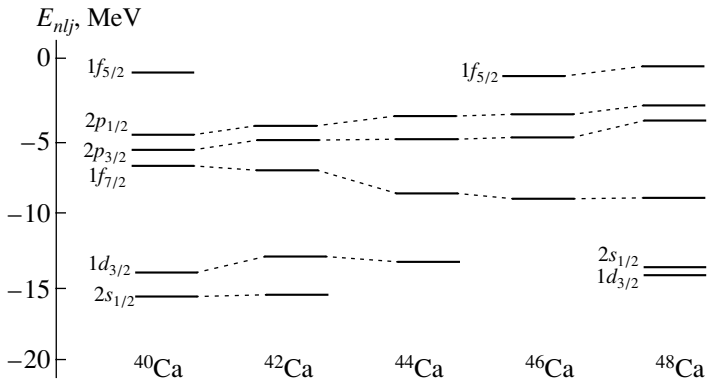

Fig. 1. Experimental values of the energies of neutron single-particle states in ^{40,42,44,46,48}Ca.

3. COMPARISON OF THE SINGLE-PARTICLE ENERGIES E_{nlj}^{expt} OF NEUTRON STATES IN ^{40,42,44,46,48}Ca WITH THE CALCULATED ENERGIES E_{nlj}^{theor}

In [34], information about E_{nlj}^{expt} for deep hole levels was obtained from an analysis of the quasielastic-deuteron-knockout reaction $^{40}\text{Ca}(p, np)^{39}\text{Ca}$ at $E_p = 1.0$ GeV. Data from [34] on E_{nlj}^{expt} for deep levels and our present data on E_{nlj}^{expt} in the vicinity of E_{F} (from Table 1) are contrasted against E_{nlj}^{theor} for ^{40}Ca in Table 3. In a great number of studies, the theoretical values E_{nlj}^{theor} were calculated either for deep hole or for valence states. The number of studies where calculations were performed for all bound states of ^{40}Ca is relatively small. Some comments on the arrangement of data in Table 3 are in order here.

In column 4, we present the values E_{nlj}^{theor} calculated with the standard Woods–Saxon (WS) potential of the shell model. The depth of the neutron–nucleus interaction potential was chosen by fitting E_{nlj}^{theor} to E_{nlj}^{expt} for states in the vicinity of the Fermi energy [35].

The energies E_{nlj}^{DOM} calculated on the basis of the dispersive optical model are given in columns 5 and 6 [31, 36]. By and large, the agreement between E_{nlj}^{DOM} and E_{nlj}^{expt} is quite good. At the same time, the value of $E_{nlj}^{\text{DOM}} = -2.73$ MeV [31] for the $1f_{5/2}$ state is in sharp contradiction with the experimental value of $E_{nlj}^{\text{expt}} = -1.46$ MeV; for the $1s_{1/2}$ state, $E_{nlj}^{\text{DOM}} = -66.12$ MeV [36], which is greater in absolute value than $E_{nlj}^{\text{expt}} = -61.5(10)$ MeV [34] by approximately 5 MeV.

Columns 7–10 display the E_{nlj}^{theor} values calculated by the Hartree–Fock (HF) method with a phenomenological effective interaction between intranuclear nucleons. This interaction differs from the interaction of two free nucleons and depends strongly on the intranuclear density. In [37], use was made of the effective Skyrme interaction (HFS). In [38], Hartree–Fock calculations were performed with a potential whose density dependence is nonlinear, while, in [39], a new set of Skyrme interaction parameters that was proposed for calculating E_{nlj}^{theor} in conventional and exotic nuclei was employed. The calculations in [28] were performed with a density-dependent effective Gogny interaction.

In column 11, we give the results of the calculations performed within the self-consistent theory of finite Fermi systems (TFFS) [40]. The effective interaction of quasiparticles was introduced there phenomenologically as well (the quoted values E_{nlj}^{theor} were calculated in [40] by using set no. 5 of the parameters of the quasiparticle Lagrangian). From a comparison of the values E_{nlj}^{theor} from [40] with the analogous values from [28, 37–39], one can see that the values E_{nlj}^{theor} calculated within the self-consistent theory of finite Fermi systems are in better agreement with E_{nlj}^{expt} than their counterparts calculated within the Hartree–Fock method by using various versions of effective density-dependent interaction. This is associated in part with the energy and velocity dependence of the effective quasiparticle interaction used in the self-consistent theory of finite Fermi systems; as a result, the mean field acting on a quasiparticle also depends on its energy and velocity within this theory.

In [24, 25, 27], the energies of single-particle levels in some spherical nuclei, including ^{40}Ca, were calculated within the relativistic mean-field approximation (RMFA). Column 12 of Table 3 gives the values E_{nlj}^{theor} from [24], since only in that study did

Table 2. Experimental values $-E_{nlj}^{\text{expt}}$ (in MeV) for ^{40,48}Ca

$2s_{1/2}$	$1d_{3/2}$	$1f_{7/2}$	$2p_{3/2}$	$2p_{1/2}$	$1f_{5/2}$	References
		^{40}Ca				
17.2(18)	15.2(20)	7.52(75)	6.10(67)	4.27(43)	1.46(20)	Our study
18.2	15.6	8.4	6.3	4.3	2.9	[29]
		8.364	6.264	4.464	1.864	[30]
18.19	15.64	8.36	6.29	4.23	2.86	[31]
18.29	15.64	8.36	5.86	4.20	1.38	[5]
18.11	15.64	8.36	6.42	4.75	3.48	[32]
18.11	15.64	8.36	6.42			[33]
		^{48}Ca				
15.07(152)	15.22(179)	10.10(101)	4.68(47)	2.87(28)	1.57(40)	Our study
12.4	12.4	9.9	5.1	3.1	1.2	[29]
12.55	12.53	9.95	5.15	3.13	1.56	[33]

Table 3. Experimental energies E_{nlj}^{expt} of single-particle neutron states along with their calculated counterparts E_{nlj}^{theor} for ^{40}Ca

Subshell	$-E_{nlj}^{\text{expt}}$, MeV		$-E_{nlj}^{\text{theor}}$, MeV								
	[34]	our study	WS [35]	DOM [36]	DOM [31]	HFS [37]	HF [38]	HFS [39]	HF [28]	TFFS [40]	RMFA [24]
1	2	3	4	5	6	7	8	9	10	11	12
$1s_{1/2}$	61.5(10)		45.61	66.12	61.00	55.33	62.20				58.15
$1p_{3/2}$	42.1(4)		33.65	43.8	41.00	39.22	42.80				40.73
$1p_{1/2}$	37.5(8)		30.84	39.12	37.00	36.08	39.00				36.01
$1d_{5/2}$	23.6(1)		21.80	22.48	22.25	23.26	24.50		23.00	19.50	23.98
$2s_{1/2}$	18.2(1)	17.2(18)	18.14	17.53	17.49	17.08	18.00	15.70	18.00	16.00	17.29
$1d_{3/2}$	15.6(1)	15.2(20)	15.64	15.79	16.08	17.53	17.70	14.60	16.00	14.60	16.36
$1f_{7/2}$		7.52(75)	8.35	8.54	8.30	8.34	8.00	9.90	9.00	9.10	8.57
$2p_{3/2}$		6.10(67)	6.44	5.59	5.65	3.02		5.50	3.90	6.80	3.74
$2p_{1/2}$		4.27(43)	4.29	4.19	4.43	1.56		3.80	1.50	4.50	2.02
$1f_{5/2}$		1.46(20)	2.72	1.50	2.73	1.21		2.60	0.30	2.40	0.23

the calculations cover all bound states of the ^{40}Ca nucleus. Only the conclusion that there is qualitative agreement between E_{nlj}^{RMFA} and E_{nlj}^{expt} can be drawn from a global analysis of the values E_{nlj}^{theor} from [24, 25, 27]. According to [41], all versions of the relativistic mean-field approximation that have been developed thus far are based on the use of energy-independent scalar and vector potentials. Therefore, the relativistic mean-field approximation provides a good description of the ground-state properties of nuclei and of the order of single-particle levels, but it is unable to describe their density in the vicinity of the Fermi energy.

In summary, we can state that, at the present time,

Table 4. Experimental energies E_{nlj}^{expt} of single-particle neutron states according to the present study along with the calculated energies E_{nlj}^{theor} for ^{42,44,46,48}Ca

$-E_{nlj}$, MeV						References
$2s_{1/2}$	$1d_{3/2}$	$1f_{7/2}$	$2p_{3/2}$	$2p_{1/2}$	$1f_{5/2}$	
			^{42}Ca			
15.44(154)	13.03(184)	7.70(107)	5.73(57)	4.10(41)		Our study
17.44	16.85	8.81	3.86	2.19	1.80	[24]
17.80	16.40	9.00	4.00	1.80	0.40	[28]
18.10	15.40	7.80	6.30	1.80	0.30	[42]
		8.80	5.60	5.60	4.00	[1]
			^{44}Ca			
17.61	13.91(159)	9.23(112)	5.92(75)	3.63(36)		Our study
	17.39	9.10	3.97	2.34	0.64	[24]
17.80	16.70	9.00	4.10	2.00	0.60	[28]
		9.00	5.20	3.70	1.00	[1]
			^{46}Ca			
17.81		10.00(100)	5.85(60)	3.58(39)	3.20(45)	Our study
	17.97	9.43	4.10	2.50	0.90	[24]
		9.20	4.30	2.20	0.80	[28]
		9.30	5.00	3.20	1.00	[1]
			^{48}Ca			
15.07(152)	15.22(179)	10.10(101)	4.68(47)	2.87(28)	1.57(40)	Our study
12.59	12.51	9.90	5.14	3.09	1.15	[37]
18.10	18.95	9.10	4.13	2.60	2.02	[39]
20.50	20.70	10.40	5.10			[35]
15.10	13.60	8.80	5.80	4.20	1.90	[38]
18.20	17.60	9.50	4.60	2.50	1.10	[28]
13.70	13.00	8.30	6.50	4.00	1.50	[40]
18.02	18.69	9.83	4.19	2.64	1.15	[24]
		9.80	5.00	3.00	1.00	[1]

the calculations within the dispersive optical model and within the self-consistent theory of finite Fermi systems lead to the best agreement between E_{nlj}^{theor} and E_{nlj}^{expt} for ^{40}Ca.

For ^{42,44,46,48}Ca, there are no data on E_{nlj}^{expt} for deep hole states. In Table 4, data available in the literature for E_{nlj}^{theor} are therefore contrasted only against the values E_{nlj}^{expt} in the vicinity of E_{F} that were found in the present study.

From the experimental and theoretical values of E_{nlj} that are presented in Table 4 for ^{42,44,46}Ca, one can see that the values E_{nlj}^{MSM} calculated in [1] exhibit

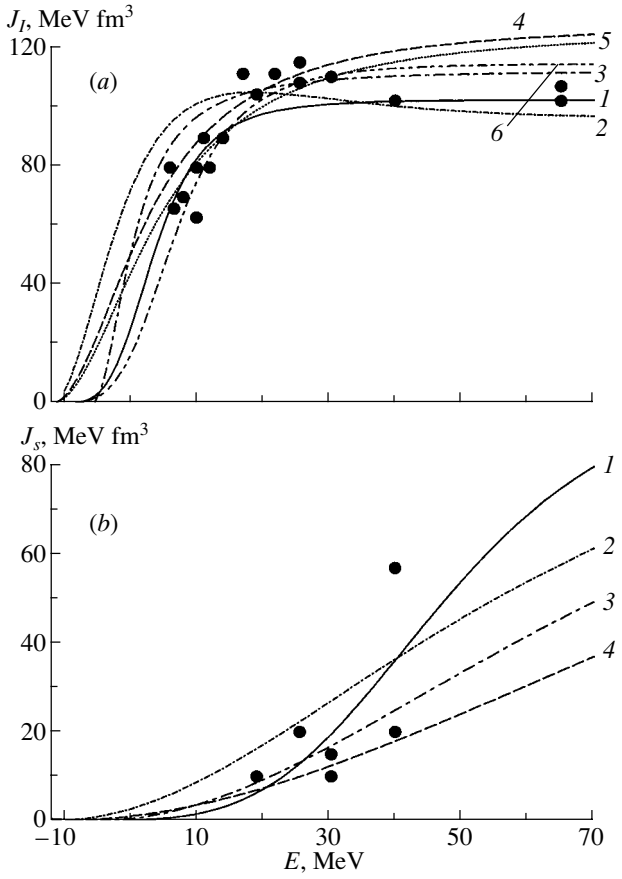

Fig. 2. (*a*) Volume integral J_I of the imaginary part of the optical potential and (*b*) volume integral J_s of the volume component of the imaginary optical potential for the $n + {}^{40}$Ca system versus energy: (points) experimental values of $J_I(E_k)$ and $J_s(E_k)$ and (curves) parametrizations of $J_I(E)$ and $J_s(E)$ (see explanations in the main body of the text).

smaller deviations from E_{nlj}^{expt} than the values E_{nlj}^{theor} from [24, 28, 42].

The values E_{nlj}^{theor} for ^{48}Ca in Table 4 were borrowed from the same articles as those for ^{40}Ca. The calculated values E_{nlj}^{TFFS} [40] and E_{nlj}^{MSM} [1] show the smallest deviations from E_{nlj}^{expt}.

Since the best agreement between E_{nlj}^{theor} and E_{nlj}^{expt} for ^{40}Ca was obtained in the case of the calculations within the dispersive optical model, it is of importance to address the following issues: the application of the dispersive optical model to describing E_{nlj}^{expt} for the ^{42,44,46,48}Ca nuclei and the investigation of the possibility of employing the dispersive optical model to calculate the single-particle energies of the bound states of neutrons in neutron-rich calcium isotopes. This is done in the sections of this article that follow.

4. ANALYSIS OF THE SINGLE-PARTICLE FEATURES OF NEUTRON STATES IN ^{40}Ca WITHIN THE DISPERSIVE OPTICAL MODEL

The method of a dispersive optical-model analysis is based on the idea to employ information about neutron (proton) scattering on a nucleus to calculate the single-particle features of neutron (proton) bound states in this nucleus. The method for calculating single-particle features of levels in spherical nuclei on the basis of the dispersive optical model was described in detail in a number of studies (see [43] and references therein).

For the $n + A$ system, the dispersive optical potential can be represented in the form

$$U(r,E) = -U_n(r,E) - U_{\text{so}}(r,E), \qquad (9)$$

where $U_n(r,E)$ is a complex-valued central potential and $U_{\text{so}}(r,E)$ is a spin–orbit potential. The central potential is the sum of three components of the real part and two components of the imaginary part; that is,

$$U_n(r,E) = V_{\text{HF}}(r,E) + \Delta V_s(r,E) \qquad (10)$$
$$+ \Delta V_d(r,E) + i[W_s(r,E) + W_d(r,E)].$$

In (10), V_{HF} is the Hartree–Fock component; $\Delta V_{s,d}$ and $W_{s,d}$ are, respectively, the dispersive and imaginary parts of the dispersive optical potential; and the indices s and d label, respectively, the volume and surface parts. Within the dispersive optical model, $\Delta V_s(r,E)$ and $\Delta V_d(r,E)$ are calculated with the aid of dispersion relations where $W_s(r,E)$ and $W_d(r,E)$ appear as integrands. The dispersion relations are also valid for the volume integrals of the corresponding parts of the dispersive optical potential.

Within the traditional version of the dispersive optical model, one analyzes experimental data on the differential cross sections $\sigma^{\text{expt}}(\theta)$ for the respective scattering process and on the corresponding polarization $P^{\text{expt}}(\theta)$ at a specific energy value E_k. Data on the volume integrals per nucleon of the resulting imaginary potentials $J_s(E_k)$, $J_d(E_k)$, and $J_I(E_k) = J_s(E_k) + J_d(E_k)$ are parametrized by analytic dependences $J_s(E)$, $J_d(E)$, and $J_I(E)$ that are symmetric with respect to E_{F}. These dependences are then used to calculate the volume integrals of the dispersive components of the dispersive optical potential.

In order to determine the parameters of the dispersive optical potential, the experimental values $\sigma^{\text{expt}}(\theta)$ and $P^{\text{expt}}(\theta)$ for the $n + {}^{40}$Ca system were analyzed in [44] for $9.9 \le E_n \le 40$ MeV, in [36] for $5.3 \le E_n \le 40$ MeV, and in [31] for $11 \le E_n \le 40$ MeV. By using the optical-potential parameters found previously by

other authors, $J_s(E_k)$, $J_d(E_k)$, and $J_I(E_k)$ were determined in [31, 36, 44]; of these, $J_s(E_k)$ and $J_I(E_k)$ are shown in Fig. 2, and they are seen to have the largest scatter.

In [44], the dependences $J_I(E_k)$ and $J_s(E_k)$ were parametrized by means of the Brown–Rho formula,

$$J_I(E) = \frac{\alpha_I}{1+\left(\frac{\beta_I}{E-E_\mathrm{F}}\right)^2}, \qquad (11)$$
$$J_s(E) = \frac{\alpha_I}{1+\left(\frac{\beta_s}{E-E_\mathrm{F}}\right)^2},$$

where α_I, β_I, and β_s are parameters.

In [31], use was made of a parametrization where E_0 was substituted for E_F in (11). It is assumed that, in the interval from E_F to E_0 and in the interval from $(2E_\mathrm{F}-E_0)$ to E_F, the imaginary potential vanishes, so that single-particle states are not fragmented.

In Fig. 2*a*, curve *3* was calculated by formula (11) with the parameters set to the values of $\alpha_I = 113.6$ MeV fm^3, $\beta_I = 6.46$ MeV, and $E_0 = -5.86$ MeV [31]; also, the parameter values used in this figure were $\alpha_I = 130$ MeV fm^3, $\beta_I = 15$ MeV, and $E_\mathrm{F} = -12.0$ MeV [36] for curve *4* and $\alpha_I = 128$ MeV fm^3, $\beta_I = 16.5$ MeV, and $E_\mathrm{F} = -12$ MeV [44] for curve *5*.

In [44], use was made of the Jeukenne–Mahaux approximating formula,

$$J_I(E) = \frac{\alpha_I}{1+\left(\frac{\beta_I}{E-E_\mathrm{F}}\right)^4}, \qquad (12)$$
$$J_s(E) = \frac{\alpha_I}{1+\left(\frac{\beta_s}{E-E_\mathrm{F}}\right)^4}.$$

Curve *6* in Fig. 2*a* was calculated by formula (12) with the parameter values of $\alpha_I = 116$ MeV fm^3, $\beta_I = 18.8$ MeV, and $E_\mathrm{F} = -12.0$ MeV [44].

In Fig. 2*a*, the point at $E_k = 65$ MeV was borrowed from data reported in [45]. This value of $J_I(E_k)$ was not taken into account in determining the parameters α_I and β_I in [31, 36, 44]. From the above list of values of the parameters α_I and β_I, one can see that they have a considerable scatter for a specific approximating dependence.

In Fig. 2*b*, curves *4* and *3* were calculated by formula (11) with the parameter values of $\alpha_I = 130$ MeV fm^3, $\beta_s = 130$ MeV, and $E_\mathrm{F} = -12.0$ MeV [36] for the former and the parameter values of $\alpha_I = 113.6$ MeV fm^3, $\beta_s = 86.5$ MeV, and $E_0 = -5.86$ MeV [31] for the latter.

In practice, the application of the above version of the dispersive optical model involves considerable difficulties because of the absence of information about $\sigma^{\mathrm{expt}}(\theta)$ and $P^{\mathrm{expt}}(\theta)$ at various values of E_k for many nuclei. This comment applies perfectly to the ^{42,44,46,48}Ca nuclei. This explains the fact that, in various studies, an analysis within the dispersive optical model was performed only for a few nuclei. The version of the dispersive optical model where the parameter α_I for the $p+A$ and $n+A$ systems is determined by the method described below was proposed in [43, 46] in order to overcome these difficulties.

In [47], the CH89 systematics of the average (global) parameters of a traditional (nondispersive) optical potential was proposed on the basis of an analysis of information about $\sigma^{\mathrm{expt}}(\theta)$ and $P^{\mathrm{expt}}(\theta)$ for $p+A$ systems in the range $16 \le E \le 65$ MeV and $n+A$ systems in the range $10 \le E \le 26$ MeV for nuclei in the mass-number range $40 \le A \le 209$. In this systematics, the strength parameters depend on E and A, the range parameters depend on A, and the diffuseness parameters of the real and imaginary potentials are fixed at $a_V = a_s = a_d = 0.69$ fm. The CH89 systematics was composed without including experimental data on the total reaction cross sections $\sigma_r(E)$. Later on, $\sigma_r(E)$ was measured for some $p+A$ systems to a precision of about 3% [48]. The $\sigma_r^{\mathrm{CH89}}(E_k)$ values calculated with the CH89 parameters agree with $\sigma_r^{\mathrm{expt}}(E_k)$ [43] to within about 15%. In [49], it was shown that, for each $p+A$ system, one can determine individual values of the parameters $a_s^* = a_d^*$ for each nucleus such that the use of these values, together with the remaining parameter values of the CH89 systematics, leads to the cross sections $\sigma_r^{\mathrm{CH89}}(E_k)$ that are consistent with $\sigma_r^{\mathrm{expt}}(E_k)$ to within 3%. The version of the CH89 systematics where, instead of the average value of $a_s = a_d = 0.69$ fm, use is made of individual parameters $a_s^* = a_d^*$ for each nucleus was denoted by CH89* in [49]. The use of individual values of $a_s^* = a_d^*$ reduces the root-mean-square deviations χ^2 of $\sigma^{\mathrm{CH89}^*}(\theta)$ and $P^{\mathrm{CH89}^*}(\theta)$ from $\sigma^{\mathrm{expt}}(\theta)$ and $P^{\mathrm{expt}}(\theta)$ to values close to those found by freely varying all parameters of the potential of the traditional optical model. The average parameters of the CH89 systematics make it possible to describe well the positions of the maxima and minima of the experimental differential cross sections for elastic scattering and of the respective polarization, but the results for their absolute values prove to be inadequate. The description of the absolute cross-section and polarization values depends predominantly on the imaginary part of the optical potential; in order to improve this description, it is

necessary to go over from the average values of the geometric parameters of the imaginary part of the optical potential for all nuclei to individual parameters for each nucleus. It turned out that this individualization can be implemented by varying only the parameters $a_s = a_d$. The use of the CH89* systematics of parameters underlies the dispersive-optical-model version developed in [43]. Within this version, a subsequent determination of the parameters of the dispersive optical potential is based on analyzing the model dependences $\sigma^{\mathrm{CH89^*}}(\theta)$ and $P^{\mathrm{CH89^*}}(\theta)$ instead of $\sigma^{\mathrm{expt}}(\theta)$ and $P^{\mathrm{expt}}(\theta)$. In [43, 46], it was shown that, for $p + A$ systems, the procedure for determining the average parameters of the dispersive optical potential is simplified considerably within this version without loss of accuracy.

In the CH89 systematics, the geometric parameters of the optical potential are identical for $p + A$ and $n + A$ systems. In the CH89* systematics, the parameters $a_s^* = a_d^*$ take individual values for each $p + A$ system. There arises the question of whether the parameters $a_s^* = a_d^*$ found for $p + A$ systems are appropriate for $n + A$ systems. In [50], it was shown that the values of $a_s^* = a_d^*$ make it possible to describe experimental data on $\sigma(\theta)$, the total reaction cross sections σ_r, and the total interaction cross sections σ_t for $n + A$ systems as well.

A new global systematics of the parameters of the traditional optical potential was proposed in [51], and individual (local) parameters were determined there for some nuclei. The values of the parameter α_I that were obtained from an analysis of the model cross sections $\sigma^{\mathrm{CH89^*}}(\theta)$ and $\sigma^{[51]}(\theta)$ for calcium isotopes differ from one another within 2 to 3%. In the present study, the volume integrals $J_s^{\mathrm{CH89^*}}(E)$ and $J_I^{\mathrm{CH89^*}}(E)$ are approximated by the expressions in (12), where $\alpha_I = J_I^{\mathrm{CH89^*}}(E_k)$ for $E_k \approx$ 50–60 MeV.

In order to determine the parameter β_I, one needs experimental information about $\sigma^{\mathrm{expt}}(\theta)$ and $P^{\mathrm{expt}}(\theta)$ at low energies. Since there are no such data for even–even calcium isotopes, with the exception of ^{40}Ca, it would be reasonable to determine β_I in (12) as an adjustable parameter that corresponds to the minimum deviation of the energies E_{nlj}^{DOM} calculated within the dispersive optical model from E_{nlj}^{expt} in the vicinity of E_{F}.

In order to determine β_s within the traditional version of the dispersive optical model, it is necessary to have information about the values of $J_s(E_k)$ for $E_k \approx$ 30–60 MeV. Because of the aforementioned scarcity of experimental information, the parameter β_s was found here on the basis of data on $J_s(E_k = E_{\mathrm{F}} - E_{1s1/2})$ from the systematics presented in [47, 51]. In doing this, it was assumed that $E_{1s1/2} \approx -60$ MeV.

For ^{40}Ca, the parameter α_I, which appears in (12), was determined in this study to be 103.5 MeV fm^3. Curve *1* in Fig. 2*a* was calculated by using this value of the parameter α_I, $E_{\mathrm{F}}^{\mathrm{expt}} = -11.36$ MeV, and $\beta_I =$ 18 MeV. From Fig. 2*a*, one can see that curve *1* is consistent with the empirical values of $J_I(E_k)$ at $E_k \leq 10$ MeV and $E_k = 40$ and 65 MeV. In the region of low energies, the dependence $J_I(E)$ calculated with the parameters of the systematics from [51] (curve *2*) agrees poorly with $J_I(E_k)$.

In Fig. 2*b*, curve *1* was calculated by formula (12) with the parameter values of $\alpha_I = 103.5$ MeV fm^3, $\beta_s = 65$ MeV, and $E_{\mathrm{F}}^{\mathrm{expt}} = -11.36$ MeV; for curve *2*, use was made of the parameters from [51].

Within the traditional version of the dispersive optical model, the geometric parameters $r_{s,d}(E_k)$ and $a_{s,d}(E_k)$ are found from an analysis of $\sigma^{\mathrm{expt}}(\theta)$ and $P^{\mathrm{expt}}(\theta)$ under the condition that the volume integrals $J_{s,d}(E_k)$ are fixed in accordance with an analytic dependence chosen for them (in the Jeukenne–Mahaux, the Brown–Rho, or some other form). After that, the parameters $r_{s,d}(E_k)$ and $a_{s,d}(E_k)$ are averaged over energy. In [43, 46], it was shown that the parameters of the CH89* systematics can be taken for the average parameters r_s, r_d, a_s, and a_d.

A method for determining the energy dependence of the strength parameter of the Hartree–Fock component $V_{\mathrm{HF}}(E)$ was proposed in [43, 46]. As in [43], the dependence $V_{\mathrm{HF}}(E)$ was represented here as

$$V_{\mathrm{HF}}(E) = V_{\mathrm{HF}}^{(1)}(E_{\mathrm{F}}) + V_{\mathrm{HF}}^{(2)}(E_{\mathrm{F}})\exp\left[\frac{-\lambda(E - E_{\mathrm{F}})}{V_{\mathrm{HF}}^{(2)}(E_{\mathrm{F}})}\right] \text{ for } E > E_{\mathrm{F}} \quad (13)$$

and as

$$V_{\mathrm{HF}}(E) = V_{\mathrm{HF}}(E_{\mathrm{F}}) - \lambda(E - E_{\mathrm{F}}) \text{ for } E < E_{\mathrm{F}}, \quad (14)$$

where

$$V_{\mathrm{HF}}(E_{\mathrm{F}}) = V_{\mathrm{HF}}^{(1)}(E_{\mathrm{F}}) + V_{\mathrm{HF}}^{(2)}(E_{\mathrm{F}}). \quad (15)$$

The parameters $V_{\mathrm{HF}}(E_{\mathrm{F}})$, λ, r_{HF}, and a_{HF} were determined according to the following procedure. The dispersive components of the real part of the dispersive optical potential (10), $\Delta V_s(r, E)$ and $\Delta V_d(r, E)$, were calculated with the parameters α_I, β_I, β_s, r_s, r_d, a_s, and a_d fixed at the values found for them. The parameters r_{so} and a_{so} were taken in accordance with [47] or [51], while the parameter V_{so} was varied.

It turned out that, to within 3%, the $J_{\mathrm{HF}}(E_{\mathrm{F}})$ and $V_{\mathrm{HF}}(E_{\mathrm{F}})$ values determined within various versions

Table 5. Parameters of the dispersive optical potential for the $n + {}^{40-56}$Ca systems

A	$r_d = r_s$, fm	$a_d = a_s$, fm	α_I, MeV fm^3	β_s, MeV	β_I, MeV	r_{so}, fm	a_{so}, fm	r_{HF}, fm	a_{HF}, fm	λ	$-E_F$, MeV	V_{so}, MeV fm^3
40	1.207	0.600	103.5	60	18	0.989	0.63	1.179	0.79	0.580	11.36	5.9
42	1.209	0.605	88	60	9	0.995	0.63	1.160	0.760	0.561	10.36	6.2
44	1.211	0.610	90	60	12	1.000	0.63	1.190	0.667	0.572	11.57	6.5
46	1.213	0.615	90	60	12	1.005	0.63	1.200	0.636	0.577	12.3	6.8
48	1.214	0.540	83	54	15	1.010	0.63	1.205	0.619	0.557	7.4	7.0
50	1.216	0.53	80	53	18	1.014	0.63	1.170	0.760	0.576	7.2	7.2
52	1.217	0.54	80	53	18	1.018	0.63	1.150	0.850	0.563	2.2	7.5
54	1.217	0.54	80	53	18	1.018	0.63	1.150	0.850	0.579	2.2	8.0
56	1.220	0.53	80	53	15	1.026	0.63	1.150	0.850	0.573	2.3	8.0

of the dispersive optical model for various $n + A$ and $p + A$ systems agree with the $J_V^{[51]}(E_F)$ and $V^{[51]}(E_F)$ values calculated by the formulas from [51]. We note that the identity $J_{HF}(E_F) \equiv J_V(E_F)$ holds by definition of the dispersion relations (see [52]). This made it possible to determine, for each trial value of r_{HF}, the corresponding diffuseness parameter a_{HF} from the equality $g_{HF} = g_V^{[51]}$, where

$$g_{HF} = \int f(r, r_{HF}, a_{HF}) d\mathbf{r}, \qquad (16)$$
$$g_V^{[51]} = \int f(r, r_V^{[51]}, a_V^{[51]}) d\mathbf{r}.$$

For several fixed values of V_{so} and trial pairs of r_{HF} and a_{HF}, the values of $V_{HF}(E_{nlj})$ were found from a fit to $E^{expt}_{1s1/2}$, $E^{expt}_{1d3/2}$, and $E^{expt}_{1f7/2}$ in solving the Schrödinger equation for bound states. The parameters $V_{HF}(E_F)$ and λ, which appear in (13) and (14), were determined for ^{40}Ca by the formulas

$$V_{HF}(E_F) = \frac{V_{HF}(E^{expt}_{1d3/2}) + V_{HF}(E^{expt}_{1f7/2})}{2}, \qquad (17)$$

$$\lambda = \frac{V_{HF}(E^{expt}_{1s1/2}) - V_{HF}(E_F)}{E^{expt}_{1s1/2} - E^{expt}_F}. \qquad (18)$$

The energies E^{DOM}_{nlj} for the $2s_{1/2}$, $1d_{3/2}$, $1f$, and $2p$ states in the vicinity of E_F were calculated by the iteration method (for details of the relevant calculation, the interested reader is referred to [43]) in solving the Schrödinger equation at fixed values of the dispersive-optical-potential parameters V_{so}, r_{so}, a_{so}, $V_{HF}(E_F)$, λ, r_{HF}, and a_{HF}. The optimum set of trial parameters was determined by minimizing the functional

$$\chi^2 = \sum_{nlj} \left(\frac{E^{DOM}_{nlj} - E^{expt}_{nlj}}{\Delta^{expt}_{nlj}} \right)^2.$$

The values found in this way for the parameters of the dispersive optical potential are given in Table 5.

The criterion according to which the parameters of the dispersive optical potential are self-consistent if, in the energy range $E_F - 10$ MeV $< E < E_F + 10$ MeV, the volume integral ΔJ_I of the sum of the dispersive corrections ΔV_s and ΔV_d is a nearly linear function of energy was discussed in [41]. Figure 3 displays the dependences $\Delta J_{I,s,d}$, which illustrate self-consistency according to this criterion for the dispersive-optical-potential parameters given in Table 5.

The calculated values of single-particle energies E_{nlj} of states and their occupation numbers N_{nlj} (the formulas for calculating N_{nlj} can be found in [5]) are given in Table 6. Column 2 there contains the experimental values E^{expt}_{nlj} obtained in [34] for the $1s_{1/2}$–$1d_{5/2}$ states and in the present study for the $2s_{1/2}$–$1f_{5/2}$ states; columns 3 and 4 present the values E^{DOM}_{nlj} and N^{DOM}_{nlj}, respectively, calculated in the present study; and column 5 gives the values N^{expt}_{nlj} determined in the present study. In order to demonstrate the dependence of the energies E^{DOM}_{nlj} on the choice of the parameter β_I, the values E^{DOM}_{nlj} calculated at $\beta_I = 15$ MeV are quoted in column 6. The results calculated in the present study with $\beta_I = 18$ MeV correspond to the minimum of the sum of the squared deviations of E^{DOM}_{nlj} calculated in [31, 36] (see

Table 6. Experimental values of the single-particle energies E_{nlj} and of the respective occupation numbers N_{nlj} in ^{40}Ca along with their counterparts calculated on the basis of the dispersive optical model

Subshell	$-E^{\text{expt}}_{nlj}$, MeV	$-E^{\text{DOM}}_{nlj}$, MeV	N^{DOM}_{nlj}	N^{expt}_{nlj}	$-E^{\text{DOM}}_{nlj}$, MeV ($\beta_I = 15$ MeV)
1	2	3	4	5	6
$1s_{1/2}$	61.5(10)	61.47	0.934		61.35
$1p_{3/2}$	42.1(4)	40.53	0.921		40.36
$1p_{1/2}$	37.5(8)	35.30	0.915		35.00
$1d_{5/2}$	23.6(1)	21.24	0.894		20.23
$2s_{1/2}$	17.2(18)	17.61	0.891	0.67–0.79	16.80
$1d_{3/2}$	15.2(20)	15.01	0.874	0.81–0.85	14.25
$1f_{7/2}$	7.52(75)	7.72	0.113	0.02–0.04	7.36
$2p_{3/2}$	6.10(67)	5.63	0.072	0.00–0.04	5.39
$2p_{1/2}$	4.27(43)	4.08	0.060	0.00–0.06	3.93
$1f_{5/2}$	1.46(20)	1.46	0.072	0.00–0.02	1.48

Note: The values E^{expt}_{nlj} for the $1s_{1/2}$–$1d_{5/2}$ and $2s_{1/2}$–$1f_{5/2}$ states were obtained in [34] and in the present study, respectively.

Table 3, columns 6, 5) from E^{expt}_{nlj} for the $2s_{1/2}$–$1f_{5/2}$ states. We note that the values N^{DOM}_{nlj} calculated on the basis of the dispersive optical model in the present study and in [31, 36] for the $1f_{7/2}$, $2p_{3/2}$, and $1f_{5/2}$ states exceed their experimental counterparts. In [8], it was shown that the calculated values N^{DOM}_{nlj} for states in the vicinity of E_{F} can be reduced upon considering that the imaginary potential is nonlocal, which violates the symmetry of absorption with respect to E_{F} at high $|E|$.

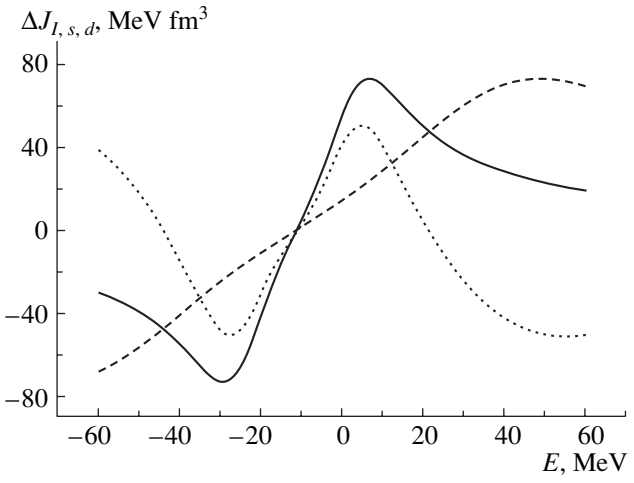

Fig. 3. Energy dependences of the volume integrals (solid curve) ΔJ_I, (dashed curve) ΔJ_s, and (dotted curve) ΔJ_d of the dispersive components of the dispersive optical potential for the $n + {}^{40}$Ca system.

The results obtained in this section provide grounds to employ the proposed version of the dispersive optical model to describe the features of single-particle states in the ^{42,44,46,48}Ca nuclei. This is done in the next section.

5. COMPARISON OF EXPERIMENTAL SINGLE-PARTICLE FEATURES OF NEUTRON STATES IN ^{42,44,46,48}Ca WITH THEIR COUNTERPARTS CALCULATED ON THE BASIS OF THE DISPERSIVE OPTICAL MODEL

In the even–even isotopes ^{42,44,46}Ca, there occurs the successive filling of the $1f$ and $2p$ subshells. In describing nuclei that involve open shells, it is necessary to take into account superfluid correlations. We assume that nucleon-pairing effects can be taken into account by selecting individual parameters of the dispersive optical potential for each nucleus. According to [53], the experimental values of the ground-state spins and parities are $7/2^-$ in ^{43,45,47}Ca and $3/2^-$ in ^{49}Ca. If use is made of the values E^{expt}_{nlj} for the $1d_{3/2}$ and $1f_{7/2}$ states in ^{42,44}Ca (see Table 1), then the average values of the Fermi energy for these two nuclei are $E_{\text{F}} = -10.36$ and -11.57 MeV, respectively. For ^{46}Ca, there are no data on the energy of the $1d_{3/2}$ state. Assuming that the average value of the

energy of the $1d_{3/2}$ state in ^{46}Ca is equal to the half-sum of the energies of the analogous states in ^{44}Ca and ^{48}Ca, we obtain, for ^{46}Ca, the average value of $E_F = -12.3$ MeV estimated on the basis of the data in Table 1. For ^{48}Ca, the data in Table 1 lead to the average value of $E_F = -7.4$ MeV, which is in good agreement with the value of -7.55 MeV found from data on the binding energies. The deviation of the E_F values calculated for ^{42,44,46}Ca by using data on the binding energies (-9.70, -9.27, and -8.84 MeV, respectively) from those determined on the basis of information about E_{nlj}^{expt} indicates that the structure of levels in these nuclei differs from the single-particle structure.

In order to determine the parameters of the dispersive optical potential for ^{42,44,46,48}Ca, we employed the dispersive-optical-model version described in the preceding section, slightly changing the procedure for evaluating the parameter V_{so}.

For a large number of magic nuclei and nuclei close to magic ones, Koura and Yamada [33] presented a compilation of the single-particle energies E_{nlj}^{expt} of proton and neutron states in a tabular form. They compared the experimental values of E_{nlj} with the theoretical results found within the relativistic mean-field approximation. The shell potential was written in the standard form by using the Woods–Saxon form factors. Expressions for calculating the parameters of the shell potential and tables of these parameters were also given in that article. We used the tables of the parameters from [33] and calculated the volume integrals of the spin–orbit potentials for ^{40}Ca and ^{48}Ca. It turned out that the volume integral for ^{48}Ca is approximately 15 to 20% greater than that for ^{40}Ca.

At the present time, the isospin dependence of the spin–orbit potential is being studied in detail by many authors. Interest in this problem was stimulated by the development of studies within the relativistic mean-field approximation (see [54–56] and references therein). However, there is no unambiguous solution here because of the scarcity of relevant experimental data.

If the geometric parameters of the spin–orbit potential are fixed, for example, in accordance with the CH89 systematics, then an increase in the volume integral for ^{48}Ca can be associated with an increase in the strength parameter V_{so}. A slight increase in V_{so} in response to a change in A from 40 to 48 can be described by using the formulas proposed in [57],

$$V_{so}^n = \frac{(NV_{nn} + ZV_{np})}{A} K \ \ [\text{MeV fm}^2], \qquad (19)$$

where

$$K = 0.263\left[1 + 2\frac{N-Z}{A}\right], \qquad (20)$$

$$V_{pp} = V_{nn} = 19.7, \quad V_{pn} = V_{np} = 87. \qquad (21)$$

It can readily be shown that, for the $n + {}^{42,44,46,48}$Ca systems, the quantity V_{so}^n can be represented in the form

$$V_{so}^n(A) = V_{so}^n(A = 40)\xi, \qquad (22)$$

where

$$\xi = 1 + 0.018(A - 40). \qquad (23)$$

For each calcium isotope, we have calculated $V_{so}^n(A)$ by formulas (22) and (23) at the fixed value of $V_{so}^n(A = 40) = 5.9$ MeV fm^2.

The parameters α_I for the $n + {}^{42,44,46,48}$Ca systems were determined by the method applied to the $n + {}^{40}$Ca system. By using data on σ_r from [48] for the $p + {}^{42,44,48}$Ca systems and the values of σ_r for ^{46}Ca that were estimated on the basis of data from [48], we determined the CH89* parameters for the $n + {}^{42,44,46,48}$Ca systems by the method proposed in [50] and found that $\alpha_I = 88$, 90, 90, and 83 MeV fm^3, respectively. If one employs data from [51], the values of the parameter α_I for these systems appear to be 93, 92, 90, and 88 MeV fm^3, respectively. The maximum distinction between the values of α_I that were determined with the parameters from [51] and from the CH89* systematics was 5%. The error of 5% in determining α_I does not have a significant effect on the accuracy in determining E_{nlj}^{DOM}. In the following, we will use the values of α_I that were calculated on the basis of the CH89* parameters.

The values of the parameters β_s were calculated, while the values of β_I, r_{HF}, and a_{HF} were selected for each $n + A$ system by using the same procedure as that which was described for the $n + {}^{40}$Ca system in Section 3. The resulting set of dispersive-optical-potential parameters for the ^{42,44,46,48}Ca nuclei is given in Table 5.

The values E_{nlj}^{DOM} calculated with the parameters from Table 5 are given in Table 7. Comparing the values E_{nlj}^{DOM} for the $2s_{1/2}$–$1f_{5/2}$ states in the ^{42,44,46,48}Ca nuclei with the data in Table 1, we can conclude that these results agree within the experimental errors. The agreement between N_{nlj}^{DOM} and N_{nlj}^{expt} for the ^{42,44,46,48}Ca nuclei is of approximately the same character as in the case of ^{40}Ca. For the $1f$ and $2p$ states, the values E_{nlj}^{DOM} agree well with the

values E_{nlj}^{MSM} from [1]. For the ^{42,44,46,48}Ca isotopes, the spin–orbit splitting $\Delta_{1p}^{\mathrm{DOM}}$ calculated on the basis of the dispersive optical model changes within the range 5.1–5.8 MeV, which is in agreement with the value of $\Delta_{1p}^{\mathrm{expt}} = 4.6(9)$ MeV for ^{40}Ca. For the $1d$ state, the values Δ_d^{DOM} range between 6.3 and 8.3 MeV, this being in agreement with the value of $\Delta_d^{\mathrm{expt}} = 8.0(2)$ MeV for ^{40}Ca. The values $\Delta_{1f}^{\mathrm{DOM}}$ and $\Delta_{2p}^{\mathrm{DOM}}$ agree with $\Delta_{1f}^{\mathrm{expt}}$ and $\Delta_{2\mathrm{p}}^{\mathrm{expt}}$, respectively, within the errors in the experimental values.

Figure 1 clearly demonstrates that, in ^{48}Ca, the filling of the $1f_{7/2}$ subshell leads to an increase in the absolute values of the energies of the respective states and that the Fermi energy E_{F} undergoes a jump upon going over from ^{46}Ca to ^{48}Ca. From Table 5, one can see that, for the $n + {}^{40,42,44,46,48}$Ca systems, all of the dispersive-optical-potential parameters, with the exception of E_{F}, take close values and that the parameter V_{so} increases smoothly. If, in calculating E_{nlj}^{DOM} for ^{48}Ca, one employs, for E_{F}, the average value for the ^{40,42,44,46}Ca isotopes, there will be no agreement between E_{nlj}^{DOM} and E_{nlj}^{expt}.

On the basis of a comparison of the results of calculations and experimental data, we can conclude that the proposed version of the dispersive optical model provides a fairly accurate description of experimental single-particle energies of bound states in calcium isotopes both for doubly magic nuclei and for nuclei featuring unfilled shells. Good agreement between E_{nlj}^{DOM} and E_{nlj}^{expt} for ^{40,42,44,46,48}Ca gives sufficient grounds to apply this version of the dispersive optical model to calculating the positions of single-particle $1f$ and $2p$ levels in ^{50,52,54,56}Ca. It would then be reasonable to compare the results derived in this way with their counterparts obtained in [1] on the basis of the multiparticle shell model. Questions associated with these calculations and comparison are considered in the next section.

6. CALCULATION OF THE SINGLE-PARTICLE ENERGIES OF NEUTRON LEVELS IN THE NEUTRON-RICH NUCLEI ^{50,52,54,56}Ca

The neutron-rich nuclei ^{50,52,54,56}Ca are unstable. They undergo beta decay, with the half-lives $T_{1/2}$ [53] being 14 s for ^{50}Ca, 4.6 s for ^{52}Ca, and 10 ms for ^{56}Ca (there are presently no data on $T_{1/2}$ for ^{54}Ca). The ground-state spin–parities determined experimentally for the ^{51}Ca and ^{53}Ca nuclei in [53] involve ambiguities, $(3/2^-)$ and $(3/2^-, 5/2^-)$, respectively. There are no data on the spins of the ^{55,57}Ca nuclei. If the spin–parity of ^{51}Ca is $3/2^-$, then $E_{\mathrm{F}} = -7.2$ MeV according to data from [1] on $E_{1f7/2}^{\mathrm{MSM}}$ and $E_{2p3/2}^{\mathrm{MSM}}$. If the spin–parity of ^{53}Ca is $3/2^-$, $E_{\mathrm{F}} = -7.35$ MeV, but, if it is $5/2^-$, then $E_{\mathrm{F}} = -2.2$ MeV. According to data from [1], E_{F} takes nearly identical values for ^{54}Ca and ^{56}Ca—they are approximately equal to -2.2 MeV.

The Δ_{1f} and Δ_{2p} values estimated for the ^{50,52,54,56}Ca nuclei on the basis of data from [1] do not decrease with increasing A, remaining approximately identical to those for ^{48}Ca. The calculations that were performed in [24] and which were based on the relativistic mean-field approximation yield, for $\Delta_{1f}^{\mathrm{RMFA}}$, values that decrease slightly with increasing A and, for $\Delta_{2\mathrm{p}}^{\mathrm{RMFA}}$, values that, on the contrary, increase slightly with increasing A. In this connection, we calculated the values of V_{so} by formulas (22) and (23) as in the case of ^{42,44,46,48}Ca.

In order to determine λ by formula (18), it is necessary to estimate the energy of the $1s_{1/2}$ state for ^{50,52,54,56}Ca. According to [24], the values $E_{1s1/2}^{\mathrm{RMFA}}$ for ^{50,52,54,56}Ca range between -58.7 and -57.4 MeV. For the ^{40}Ca nucleus, $E_{1s1/2}^{\mathrm{RMFA}} = -58.15$ MeV, but $E_{1s1/2}^{\mathrm{expt}} = -61.5(10)$ MeV. Since the average energy of this state for the ^{50,52,54,56}Ca isotopes is $E_{1s1/2}^{\mathrm{RMFA}} = -58.0$ MeV (that is, it is equal to $E_{1s1/2}^{\mathrm{RMFA}}$ for ^{40}Ca), we estimated the respective energy for them at $E_{1s1/2}^{\mathrm{est}} = -61.5(10)$ MeV. The parameters of the dispersive optical potential for ^{50,52,54,56}Ca are given in Table 5.

The calculated values E_{nlj}^{DOM} for ^{50,52,54,56}Ca are presented in Table 8. For the sake of comparison, we also quote there the respective energies calculated within the relativistic mean-field approximation [24], on the basis of the Hartree–Fock model with Skyrme forces [58], and within the multiparticle shell model [1] (E_{nlj}^{RMFA}, E_{nlj}^{HFS}, and E_{nlj}^{MSM}, respectively).

The last five columns of Table 8 display the results of the calculations based on the data of this table and performed for the energies Δ_p, Δ_d, Δ_f, and Δ_{2p} of the spin–orbit splitting of the $1p$, $1d$, $1f$, and $2p$ states and for the energy gap $\Delta = E_{1f5/2} - E_{2p1/2}$ between the $1f_{5/2}$ and $2p_{1/2}$ states.

For ^{52}Ca, Table 8 gives the calculated values E_{nlj}^{DOM} corresponding to the presumed spin–parity of the ^{53}Ca ground state, $5/2^-$.

From Table 8, one can see that the aforementioned models predict approximately identical results for the

Table 7. Single-particle neutron-state energies $-E_{nlj}^{\mathrm{DOM}}$ (in MeV) calculated for ^{42,44,46,48}Ca on the basis of the dispersive optical model with the parameter values from Table 5

A	$1s_{1/2}$	$1p_{3/2}$	$1p_{1/2}$	$1d_{5/2}$	$2s_{1/2}$	$1d_{3/2}$	$1f_{7/2}$	$2p_{3/2}$	$2p_{1/2}$	$1f_{5/2}$
42	61.55	41.31	36.16	19.79	15.69	13.52	7.59	5.52	4.06	1.52
44	61.50	42.25	36.64	21.34	16.54	14.73	8.53	5.13	3.51	1.69
46	61.63	43.07	37.28	22.37	17.05	15.40	9.52	5.46	3.72	2.18
48	61.55	43.12	37.54	24.11	17.36	15.83	9.47	5.18	3.27	1.65

Table 8. Calculated values $-E_{nlj}^{\mathrm{theor}}$ (in MeV) for ^{50,52,54,56}Ca

Subshell	DOM	RMFA	HFS	MSM	DOM	RMFA	HFS	MSM	DOM	RMFA	HFS	MSM	DOM	RMFA	HFS	MSM
	^{50}Ca				^{52}Ca				^{54}Ca				^{56}Ca			
$1s_{1/2}$	61.52	58.69			61.50	58.58			62.20	58.15			61.00	57.44		
$1p_{3/2}$	41.22	42.09			40.50	41.99			40.91	41.78			40.65	41.40		
$1p_{1/2}$	35.97	38.34			35.43	38.14			35.54	37.99			35.57	37.88		
$1d_{5/2}$	22.64	25.45			22.50	25.50			22.96	25.53			23.30	25.57		
$2s_{1/2}$	17.57	18.43			17.48	18.78			17.58	19.01			17.49	19.24		
$1d_{3/2}$	15.07	18.62			14.30	18.71			14.18	18.92			14.16	19.26		
$1f_{7/2}$	8.72	9.96	8.90	9.50	8.43	10.14	9.00	9.20	8.81	10.41	9.20	9.00	8.77	10.70	9.00	9.00
$2p_{3/2}$	5.64	4.63	5.40	5.00	5.80	5.01	5.00	5.50	5.89	5.36	4.60	6.00	5.91	5.68	4.80	6.00
$2p_{1/2}$	3.70	2.95	3.60	3.50	3.86	3.25	3.20	4.00	3.81	3.56	3.00	4.20	3.92	3.88	3.20	4.20
$1f_{5/2}$	0.90	1.53	2.00	0.70	0.67	1.92	2.20	0.50	0.50	2.37	2.50	0.30	0.84	2.90	2.60	0.50
Δ_p	5.25	3.75			5.07	3.85			5.37	3.79			5.08	3.52		
Δ_d	7.57	6.83			8.20	6.79			8.78	6.61			9.14	7.31		
Δ_f	7.82	8.43	6.90	8.80	7.76	8.22	6.80	8.70	8.31	8.04	6.70	8.70	7.93	7.80	6.40	8.50
Δ_{2p}	1.94	1.68	1.80	1.50	1.94	1.76	1.80	1.50	2.08	1.80	1.60	1.80	1.99	1.80	1.60	1.80

spin–orbit splitting of the $1f$ and $2p$ states in the ^{50,52,54,56}Ca nuclei. The predictions are substantially different for Δ. Only the values Δ^{DOM} calculated in the present study agree with Δ^{MSM} [1].

Studying in detail the question of which parameters of the dispersive optical potential are responsible above all for the agreement of E_{nlj}^{DOM} with E_{nlj}^{MSM} and of Δ^{DOM} with Δ^{MSM}, we found that, within the dispersive-optical-model version used here, these are the parameters E_{F}, r_{HF}, a_{HF}, and V_{so}. We note that this agreement takes place only at the E_{F} value from Table 5. If we fix the parameters r_{HF} and a_{HF}, then Δ^{DOM} increases with increasing V_{so}. The calculations that we performed for E_{nlj}^{DOM} at fixed values of V_{so} and various trial pairs of r_{HF} and a_{HF} (see the procedure described in Section 4) revealed that an increase in a_{HF} (accompanied by the respective slight decrease in r_{HF}) leads to the growth of Δ^{DOM}. This increase in a_{HF} (see Table 5) is consistent with the idea of the growth of the surface diffuseness of nuclei as the number N of neutrons in them increases (see, for example, [59] and articles quoted therein).

We note that, within the relativistic mean-field approximation, the energies Δ_{so} of the spin–orbit splitting of states decrease with increasing number of neutrons in neutron-rich nuclei [54–56]. Within nonrelativistic mean-field models, a spin–orbit potential is introduced as an additional parameter, and it would be natural to expect a decrease in V_{so} with increasing number of neutrons. However, it follows from the results of the present study that the dependence of V_{so} on N has some special features that call for a dedicated investigation. That such an investigation is necessary is also suggested by the results reported in [41], which show that an additional term

that takes into account the coupling between single-particle motion and collective degrees of freedom of a nucleus at energies in the vicinity of E_F must be included in the computational scheme of the relativistic mean-field approximation. In [41], this was done phenomenologically by introducing an additional potential that changes linearly with E. The introduction of such a potential leads to a change in the spin–orbit splitting of states.

Thus, the prediction of the multiparticle shell model [1] that the energy gap between the $1f_{5/2}$ and $2p_{1/2}$ levels in neutron-excess calcium isotopes must increase as the number N of neutrons increases from 28 to 34 is reproduced by the calculations within the dispersive optical model. This reproduction within a model that is different from the multiparticle shell model is an additional argument in support of the assumption put forth in [1] that the number $N = 34$ can be magic for $Z = 20$ nuclei.

7. CONCLUSIONS

(i) By using the method of matching data obtained in neutron-stripping and neutron-pickup reactions on the same nucleus, the neutron single-particle energies of valence states in the even–even isotopes $^{40-48}$Ca and their occupation numbers have been determined in the present study. The regularities of changes in the particle–hole energy gap between the $1f$ and $2p$ states of these nuclei and in the energies of their spin–orbit splitting have been investigated.

(ii) A new version of the dispersive optical model has been proposed. This version is appropriate for determining the parameters of the dispersive optical potential for $n + A$ systems, information about $p + A$ systems being partly used for this. The potential of this version of the dispersive optical model has been tested by comparing the results that it yields for the energies of single-particle neutron states in ^{40}Ca and for their occupation numbers with their experimental counterparts. It has been shown that the calculated values of these quantities are in good agreement with corresponding experimental data for the valence states of this nucleus.

(iii) On the basis of the proposed version of the dispersive optical model, we have calculated the single-particle energies of neutron states in the ^{42,44,46,48}Ca nuclei. For the valence states, the energy values calculated with the dispersive-optical-potential parameters determined individually for each nucleus have been found to agree, within the experimental errors, with the respective experimental results. This example illustrates advantages of this version of the dispersive optical model over the traditional version.

(iv) Problems associated with extrapolating the dispersive optical potential from the region of stable to the region of unstable nuclei have been investigated. The parameters of the dispersive optical potential for calculating the spectra of single-particle neutron states in the ^{50,52,54,56}Ca nuclei have been determined.

(v) Single-particle energies of neutron states in the ^{50,52,54,56}Ca nuclei have been calculated on the basis of the dispersive optical model. It has been shown that the values E_{nlj}^{DOM} for the $1f$ and $2p$ states are consistent with the values E_{nlj}^{MSM}. This result is the consequence of a slight increase in the diffuseness parameter a_{HF} (this is accompanied by a slight reduction of r_{HF}) and the strength parameter V_{so}. With increasing number of neutrons in nuclei, the energy gap Δ between the $2p_{1/2}$ and $1f_{5/2}$ states increases, reaching a maximum value at $N = 34$, this being in accord with the assumption put forth in [1] that the number $N = 34$ is magic for $Z = 20$ nuclei.

ACKNOWLEDGMENTS

This work was supported by a presidential grant (no. 1619.2003.2) for support of leading scientific schools.

REFERENCES

1. M. Honmu *et al.*, Phys. Rev. C **65**, 061301 (2002).
2. I. N. Boboshin *et al.*, Nucl. Phys. A **496**, 93 (1989).
3. M. Matoba *et al.*, Phys. Rev. C **48**, 95 (1993).
4. P. Doll *et al.*, Nucl. Phys. A **263**, 210 (1976).
5. Y. Uozumi *et al.*, Phys. Rev. C **50**, 263 (1994).
6. F. J. Eckle *et al.,* Nucl. Phys. A **506**, 159 (1990).
7. P. Martin *et al.,* Nucl. Phys. A **185**, 465 (1972).
8. G. Brown, A. Denning, and J. G. B. Haigh, Nucl. Phys. A **225**, 267 (1974).
9. T. A. Belote, W. E. Dorenbusch, and J. Rapaport, Nucl. Phys. A **120**, 401 (1968).
10. W. E. Dorenbusch, T. A. Belote, and O. Hansen, Phys. Rev. **146**, 734 (1966).
11. H. Schar, D. Trautmann, and E. Baumgartner, Helv. Phys. Acta **50**, 29 (1977).
12. J. Rapaport, W. E. Dorenbusch, and T. A. Belote, Phys. Rev. **156**, 1255 (1967).
13. J. L. Yntema, Phys. Rev. C **4**, 1621 (1971).
14. J. H. Bjerregaard, O. Hansen, and G. R. Satchler, Phys. Rev. **160**, 889 (1967).
15. J. Rapaport, W. E. Dorenbusch, and T. A. Belote, Nucl. Phys. A **177**, 307 (1971).
16. T. A. Belote *et al.,* Phys. Rev. **142**, 624 (1966).
17. J. H. Bjerregaard, O. Hansen, and G. Sidenius, Phys. Rev. **138**, 1097 (1965).
18. R. Abegg, J. D. Hutton, and M. E. Williams-Norton, Nucl. Phys. A **303**, 121 (1978).
19. W. D. Metz, W. D. Callender, and C. K. Bockelman, Phys. Rev. C **12**, 827 (1975).

20. J. S. Hanspal *et al.*, Nucl. Phys. A **436**, 236 (1985).
21. S. Fortier, E. Hourani, M. N. Rao, and S. Gales, Nucl. Phys. A **311**, 324 (1978).
22. Y. Uozumi *et al.*, Nucl. Phys. A **576**, 123 (1994).
23. T. W. Burrows, Nucl. Instrum. Methods Phys. Res. A **286**, 5953 (1990).
24. S. Typel and H. H. Wolter, Nucl. Phys. A **656**, 331 (1999).
25. M. Rashdan, Phys. Rev. C **63**, 044303 (2001).
26. B. F. Gibson and K. J. Van Oostum, Nucl. Phys. A **90**, 159 (1967).
27. K. Rutz *et al.*, Nucl. Phys. A **634**, 67 (1998).
28. M. Kleban *et al.*, Phys. Rev. C **65**, 024309 (2002).
29. X. Campi and D. W. Sprung, Nucl. Phys. A **194**, 401 (1972).
30. V. K. B. Kota and V. Potbhare, Nucl. Phys. A **331**, 93 (1979).
31. C. Mahaux and R. Sartor, Nucl. Phys. A **528**, 253 (1991).
32. L. Corradi *et al.*, Phys. Rev. C **61**, 024609 (2000).
33. H. Koura and M. Yamada, Nucl. Phys. A **671**, 96 (2000).
34. S. S. Volkov *et al.*, Yad. Fiz. **52**, 1339 (1990) [Sov. J. Nucl. Phys. **52**, 848 (1990)].
35. S. Kamerdzhiev, J. Speth, and G. Tertychny, Nucl. Phys. A **624**, 328 (1997).
36. C. H. Johnson and C. Mahaux, Phys. Rev. C **38**, 2589 (1988).
37. D. Vautherin and D. M. Brink, Phys. Rev. C **5**, 626 (1972).
38. J. W. Enlers and S. A. Moszkowski, Phys. Rev. C **6**, 217 (1972).
39. B. A. Brown, Phys. Rev. C **58**, 220 (1998).
40. V. A. Khodel and E. E. Saperstein, Phys. Rep. **92**, 183 (1982).
41. D. Vretenar, T. Nikšić, and P. Ring, Phys. Rev. C **65**, 024321 (2002).
42. P. Von Neumann-Cosel *et al.*, Nucl. Phys. A **516**, 385 (1990).
43. E. A. Romanovsky *et al.*, Yad. Fiz. **63**, 468 (2000) [Phys. At. Nucl. **63**, 399 (2000)].
44. C. Mahaux and R. Sartor, Nucl. Phys. A **484**, 205 (1988).
45. E. L. Hjort *et al.*, Phys. Rev. C **50**, 275 (1994).
46. O. V. Bespalova *et al.*, Yad. Fiz. **66**, 673 (2003) [Phys. At. Nucl. **66**, 644 (2003)].
47. R. L. Varner *et al.*, Phys. Rep. **201**, 57 (1991).
48. R. F. Carlson, At. Data Nucl. Data Tables **63**, 93 (1996).
49. E. A. Romanovsky *et al.*, Yad. Fiz. **61**, 37 (1998) [Phys. At. Nucl. **61**, 32 (1998)].
50. O. V. Bespalova *et al.*, Izv. Akad. Nauk, Ser. Fiz. **67**, 62 (2003).
51. A. J. Koning and J. P. Delaroche, Nucl. Phys. A **713**, 231 (2003).
52. C. Mahaux and R. Sartor, Adv. Nucl. Phys. **20**, 1 (1991).
53. Nuclear Wallet Cards (Jan. 2000).
54. H. Sagawa and S. Yoshida, Nucl. Phys. A **688**, 755 (2001).
55. F. Hofmann, C. M. Keil, and H. Lenske, Phys. Rev. C **64**, 034314 (2001).
56. N. Kaiser, Nucl. Phys. A **720**, 157 (2003).
57. V. A. Chepurnov, Yad. Fiz. **6**, 955 (1967) [Sov. J. Nucl. Phys. **6**, 696 (1967)].
58. B. A. Brown and W. A. Richter, Phys. Rev. C **58**, 2099 (1998).
59. J. Dobaczewski *et al.*, Phys. Rev. Lett. **72**, 981 (1994).

Translated by A. Isaakyan